

UNIVERSITY OF PATRAS - SCHOOL OF ENGINEERING
DEPARTMENT OF ELECTRICAL AND COMPUTER ENGINEERING



**ΠΑΝΕΠΙΣΤΗΜΙΟ
ΠΑΤΡΩΝ**
UNIVERSITY OF PATRAS

DIVISION: SYSTEMS AND AUTOMATIC CONTROL

THESIS

of the student of the Department of Electrical and Computer Engineering of the School of
Engineering of the University of Patras

KARADIMOS ALEXIOS OF LOUKAS

STUDENT NUMBER: 1046820

Subject

**Robotic surgical tool manipulator - Recognition,
control and manipulation of laparoscopic tools**

Supervisor

Associate Professor Dr. Evangelos Dermatas

Co-Supervisor

Professor Dr. Anthony Tzes

Thesis Number:

Patras, 2020

ΠΙΣΤΟΠΟΙΗΣΗ

Πιστοποιείται ότι η διπλωματική εργασία με θέμα

Robotic surgical tool manipulator - Recognition, control and manipulation of laparoscopic tools

του φοιτητή του Τμήματος Ηλεκτρολόγων Μηχανικών και Τεχνολογίας Υπολογιστών

Karadimos Alexios of Loukas

(A.M.: 1046820)

παρουσιάστηκε δημόσια και εξετάστηκε στο τμήμα Ηλεκτρολόγων Μηχανικών και Τεχνολογίας Υπολογιστών στις

— / — / —

Ο Επιβλέπων

Ο Διευθυντής του Τομέα

Evangelos Dermatas
Associate Professor Dr.

Kazakos Demosthenes
Assistant Professor Dr.

CERTIFICATION

It is certified that the Thesis with Subject

Robotic surgical tool manipulator - Recognition, control and manipulation of laparoscopic tools

of the student of the Department of Electrical and Computer Engineering

Karadimos Alexios of Loukas

(R.N.: 1046820)

Was presented publicly and defended at the Department of Electrical and Computer
Engineering at

— / — / —

The supervisor

The Director of the Division

Evangelos Dermatas
Associate Professor Dr.

Kazakos Demosthenes
Assistant Professor Dr.

Thesis details

Subject: **Robotic surgical tool manipulator - Recognition, control and manipulation of laparoscopic tools**

Student: **Karadimos Alexios of Loukas**

Supervising Team:

Associate Professor Dr. Evangelos Dermatas, University of Patras
Professor Dr. Anthony Tzes, NYU Abu Dhabi

Thesis research period:

Abstract

Sunt proident ut incidunt veniam ad excepteur aute nostrud. Anim nulla magna proident dolore non laboris deserunt irure. Aliqua velit quis labore quis nisi. Adipisicing amet dolor officia est ex nulla enim anim minim laboris nisi adipisicing cupidatat. Ut do consequat est ad sint dolore. Eiusmod ipsum nulla do aute culpa ad veniam eu in sunt qui laboris. Ea exercitation et quis fugiat.

Περίληψη

Sunt proident ut incidunt veniam ad excepteur aute nostrud. Anim nulla magna proident dolore non laboris deserunt irure. Aliqua velit quis labore quis nisi. Adipisicing amet dolor officia est ex nulla enim anim minim laboris nisi adipisicing cupidatat. Ut do consequat est ad sint dolore. Eiusmod ipsum nulla do aute culpa ad veniam eu in sunt qui laboris. Ea exercitation et quis fugiat.

Acknowledgements

Sunt proident ut incidunt veniam ad excepteur aute nostrud. Anim nulla magna proident dolore non laboris deserunt irure. Aliqua velit quis labore quis nisi. Adipisicing amet dolor officia est ex nulla enim anim minim laboris nisi adipisicing cupidatat. Ut do consequat est ad sint dolore. Eiusmod ipsum nulla do aute culpa ad veniam eu in sunt qui laboris. Ea exercitation et quis fugiat.

Contents

Contents	8
1 Introduction	10
1.1 Surgical robotics	10
1.1.1 Historical Overview of Surgical robotics	10
1.1.2 Surgical Robotics Procedure	12
1.1.3 Advantages & Disadvantages of Surgical robotics	13
1.2 Problem statement	14
1.3 Bibliography Overview	14
1.4 Methodology & Approach	14
2 Robotic arm Kinematic Analysis	15
2.1 Robotic arm, DH parameters & Forward Kinematics	15
2.2 Inverse Kinematics	15
2.2.1 Decoupling Technique	15
2.2.2 Workspace constraints & Singularity points	17
2.2.3 Solutions for 7DoF numerically	17
2.2.4 Comparison of Inverse Kinematics Techniques	18
3 Grasping	18
3.1 Gripper & Forward Kinematics	18
3.2 Gripper Inverse Kinematics	18
3.3 Force closure	19
3.4 Firm grasping algorithm & Force control	19
4 Scene and object recognition with Computer Vision	19
4.1 Laparoscopic tool detection	20
4.2 Stereoscopic vision	21
4.3 Calculation of tool position and orientation	21
4.4 Calculation of grasping points	22
4.5 Trocar detection & Estimation of fulcrum point	22
5 Laparoscopic tool manipulation	23
5.1 Tool pose	23
5.2 Pivoting motion with respect to Fulcrum Point	24
5.2.1 Circular trajectory of tool tip	24
5.2.2 Circular arc trajectory of tool tip	25
5.2.3 Line segment trajectory of tool tip	25
5.3 Task space analysis	26
6 Path Planning	26
6.1 Sampling methods	26
6.1.1 RRT Algorithms	26
6.1.2 PRM Algorithms	27
6.2 Pick and place algorithm	28
7 Trajectory Planning	29
7.1 Trajectory planning in cartesian coordinates	29
7.2 Trajectory planning in joint angles space	30

8 Implementation with the ROS framework	30
8.1 Introduction to the ROS framework	30
8.2 Gazebo simulation environment	31
8.3 Visualization with RViz	32
8.4 Motion Planning with Moveit	33
8.5 Experiments and Development methodology	34
8.5.1 Robot Planner 1	34
8.5.2 Robot Planner 2	35
8.5.3 Robot Planner 3	37
8.5.4 Robot Planner 4	37
8.5.5 Robot Planner 5	37
9 Results and Future Work	37
9.1 Results	37
9.2 Conclusions & Comparison with similar projects	37
9.3 Future Work	37
Appendices	38
A Software and Documentation	38
B Mathematics	38
B.1 Euler angles to Quaternions	38
Nomenclature	39
List of Figures	41
List of Figures	41
List of Algorithms	41
Bibliography	42

1 Introduction

1.1 Surgical robotics

1.1.1 Historical Overview of Surgical robotics

Surgical robotics is a field of Surgery where the surgeon operates on the patient via a computer, specialised equipment and robotic arms, to which the surgical tools needed for the operation are attached. According to surgical bibliography, robotics and laparoscopic procedures are used in general surgery, cardiothoracic surgeries, colon surgeries, gynecology, neurosurgery and orthopedics.

Robotic mechanisms were first introduced in Medicine, in 1987 with the first laparoscopic surgery of a cholecystectomy. Since then numerous laparoscopic operations have been performed and there has been a lot of improvements and innovations in this field. Such surgical operations are characterised as **minimally invasive**, because the surgical incisions made at the patient are very small and thus the probability of infection of the patient during or after the operation are very small, the hospitalization time is reduced (which means mean better and more efficient use of hospital resources) and the overall recovery of the patient is significantly faster and less painful.

However, traditional laparoscopic mechanisms have some downsides as well. First of all, the surgeon should operate in a mirrored-way, meaning that they should move at the opposite direction from what they saw at the screen (this effect is also known as the **fulcrum effect**), in order to reach the desired point of operation. Earlier laparoscopic tools had less degrees of freedom, which means less flexibility in motion control. Moreover these systems provided limited touch sensibility and feedback to the doctor they were very susceptible to the surgeon's micro movements and tremble.

The first application of robotics in Surgery appears in 1985, when Kwoh et al. [47] used a **PUMA 560**, a standard industrial robotic arm, to perform a neurosurgical biopsy, where the biopsy needle was inserted in the brain and guided with the help of Computed Tomography. This successful application was followed by the **PROBOT** surgical robot [35], which was developed at the Imperial College and used in a prostatectomy operation. Another example of an early surgery robot was the **ROBODOC** system [6] developed by Integrated Surgical Supplies in Sacramento California, which was the first to be used in orthopedics for a hip replacement surgery and was also the first to be approved by the FDA (Food & Drug Administration, organization responsible for medical devices, drugs etc.).



Figure 1: The PUMA 560 robotic arm, which was the first to be used in surgery robotics in 1985

Some other important surgery robots are listed below:

- **AESOP®Endoscope Positioner:** A voice controlled endoscopic system
- **HERMES®Control Center**

- **daVinci Surgical System®:** One of the most popular surgery robots and most used in hospitals. It is a master-slave system, which means that the operation commands are sent unidirectionally from the master console, which is controlled by the surgeon, and are executed by the robot. It also comes with a high definition 3D video feed and advanced manipulator system, one for each hand, called EndoWrist®. It is officially approved by the FDA for laparoscopic surgeries.

- **SOCRATES Robotic Telecollaboration System**

- **Raven-II [22]:** An open platform for collaborative research on surgical robotics.

- **Monarch™ Platform** by Auris Health Inc., an endoscopic system for robotic-assisted bronchoscopy



Figure 2: DaVinci Xi, ©2020 Intuitive Surgical, Inc. Patient Cart with the robotic arms that control the surgical tools



Figure 3: The MonarchTM Platform endoscopic system ¹

1.1.2 Surgical Robotics Procedure

The robotic surgery procedure starts with total anesthesia of the patient. Then the surgeon makes small incisions at the anatomical region of interest, where the procedure will take place. Through these small incisions special tubes, called trocars, are mounted, through which the laparoscopic tools are inserted. After the patient is prepared and after the patient cart, which carries the robotic arms, is successfully positioned and calibrated, the surgeon sits on a console, from where they control the robot via special sensitive joysticks. The surgeon has vision access (often in 3D) to the surgical site via a small endoscopic camera and the video is displayed on the console. In some cases, the surgeon gets force feedback from the joysticks via haptic mechanisms. Haptic force feedback is very important for the doctor in order to have a better sense of the anatomy and the surgical site, and it has gained a lot of interest in the research community.

¹<https://www.aurishealth.com/patients/robotic-bronchoscopy-patient-about-monarch-platform>



Figure 4: DaVinci Xi ©2020 Intuitive Surgical, Inc. Surgeon Console ²

1.1.3 Advantages & Disadvantages of Surgical robotics

Surgical robotics have a huge impact in Medicine and Healthcare in general. Some of the advantages are the following:

- **Minimally Invasive Procedures** which means
 - Smaller incisions
 - Less blood loss
 - Reduced risk of inpatient infection
 - Less pain
 - Faster patient recovery
- Increased **precision** and reduced human errors
 - Smooth and precise movements
 - Detection and correction of errors caused by hand tremble
- **No fulcrum effect** and intuitive manipulation of surgical tools
- **Haptic feedback.** This technology uses small mechanical forces and vibrations to give the user the sense of touch or force. Force feedback gives the ability to the surgeon to understand the mechanical properties of the tissue they operate on, such as resistance and elasticity, and thus distinguish between healthy from unhealthy tissue
- **Teleoperation** (currently in the same room only): the surgeon operates while they sit on a special **ergonomic** console, which makes the long procedures more comfortable and efficient.

²<https://www.intuitive.com/en-us/about-us/press/press-resources>

1.2 Problem statement

The goal of this thesis is to design the kinematic models and algorithms necessary for a robotic arm to detect, pick and manipulate a laparoscopic surgical tool. To achieve these goals the robotic arm must successfully do the following:

- Use computer vision to detect the scene and laparoscopic tools and with the help of stereoscopic vision, calculate the position and orientation of the center of mass of each tool, with respect to the universal reference frame
- Calculate the contact points on the tool, on which the fingers of the gripper will be placed, so that there is a firm grasp (force closure)
- Calculate the path from the tools' table to the surgical site table
- Calculate the trajectory that needs to be executed when the tool is inserted in the trocar. This is a special type of trajectory, because the motion is constrained and is known in the bibliography as a **Remote Center of Motion** (RCM) control. The constraint is that, at each time one point of the inserted tool must coincide with the RCM point (this point will also be referenced in this thesis as the center of the trocar, or the fulcrum reference frame point).

1.3 Bibliography Overview

1.4 Methodology & Approach

Column	Records
TODO	27
DOING	6
TESTING	3
DONE	9
CANCELLED	1

Figure 5: Kanban view of backlog tasks to organize all features, requirements and tasks needed to complete this thesis. The tool used to keep track of all tasks is Airtable

2 Robotic arm Kinematic Analysis

2.1 Robotic arm, DH parameters & Forward Kinematics

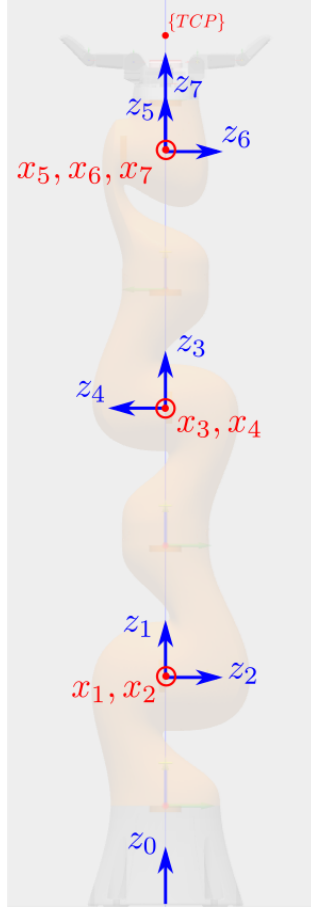


Figure 6: Joint reference frames of the KUKA iiwa14 robot

i	θ_i (rad)	L_{i-1} (m)	d_i (m)	α_{i-1} (rad)
1	θ_1	0	0.36	0
2	θ_2	0	0	$-\pi/2$
3	θ_3	0	0.36	$\pi/2$
4	θ_4	0	0	$\pi/2$
5	θ_5	0	0.4	$-\pi/2$
6	θ_6	0	0	$-\pi/2$
7	θ_7	0	0	$\pi/2$

$${}^{i-1}T_i = \begin{bmatrix} c\theta_i & -s\theta_i & 0 & L_{i-1} \\ s\theta_i c a_{i-1} & c\theta_i c a_{i-1} & -s a_{i-1} & -s a_{i-1} d_i \\ s\theta_i s a_{i-1} & c\theta_i s a_{i-1} & c a_{i-1} & c a_{i-1} d_i \\ 0 & 0 & 0 & 1 \end{bmatrix}$$

2.2 Inverse Kinematics

2.2.1 Decoupling Technique

In this section the inverse kinematics problem is solved for only the 6 out of the 7 total degrees of freedom. The third joint is not used in this analysis and its angle is set to zero $\theta_3 = 0$. The rest of the joints form a special kind of kinematic chain that can be solved using the decoupling technique. In

In this technique the Inverse kinematics problem is split to 2 separate subproblems, one for the position and one for the orientation of the end-effector. This technique can be applied in this case because the axes of the 3 last joints intersect at the same point and they form an Euler wrist.

To solve for the joints' angles, the transformation matrix 0T_7 of the end-effector with respect to the robot's base is required. Usually the transformation ${}^U T_{tcp}$ is known, which is the pose of Tool's center point (TCP) with respect to the Universal Coordinate Frame $\{U\}$ from which the required 0T_7 can be calculated

$$\begin{aligned} {}^U T_{tcp} &= {}^U T_0 \ {}^0 T_7 \ {}^7 T_{tcp} \\ {}^0 T_7 &= {}^U T_0^{-1} \ {}^U T_{tcp} \ {}^7 T_{tcp}^{-1} \\ {}^0 T_7 &= \begin{bmatrix} R_t & \mathbf{p}_t \\ 0 & 1 \end{bmatrix} \end{aligned}$$

where ${}^U T_0$, ${}^7 T_{tcp}$ are translation transformations by a constant distance and R_t , \mathbf{p}_t are the target's orientation and position respectively.

$$\begin{aligned} {}^0 \mathbf{p}_5 &= {}^0 T_4 {}^4 \mathbf{p}_5 = \begin{bmatrix} p_x \\ p_y \\ p_z \end{bmatrix} \\ \theta_1 &= \begin{cases} \text{atan2}(p_y, p_x) \\ \pi - \text{atan2}(p_y, p_x) \end{cases} \quad (2.2.1) \end{aligned}$$

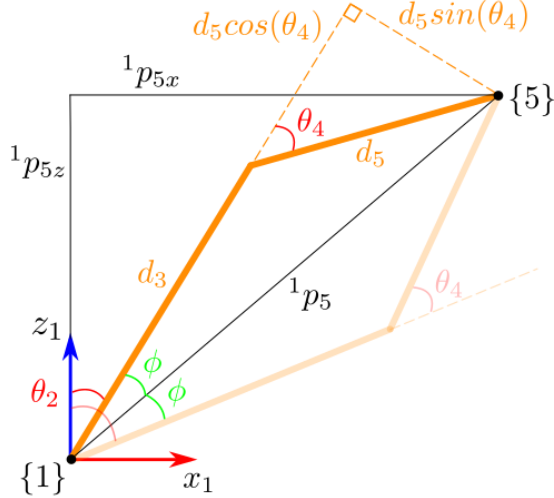


Figure 7: Calculation of angles θ_2, θ_4

$$\begin{aligned} \varphi &= \text{acos} \left(\frac{d_3^2 + \|{}^1 p_5\|^2 - d_5^2}{2d_3 \|{}^1 p_5\|} \right) \\ \theta_2 &= \text{atan2} \left(\sqrt{p_x^2 + p_y^2}, {}^1 p_{5z} \right) \pm \varphi \quad (2.2.2) \end{aligned}$$

$$c_4 = \frac{\|{}^1 p_5\|^2 - d_3^2 - d_5^2}{2d_3 d_5}$$

$$\theta_4 = \text{atan}2\left(\pm\sqrt{1 - c_4^2}, c_4\right) \quad (2.2.3)$$

Once $\theta_1, \theta_2, \theta_3, \theta_4$ are known, the orientation matrix of the wrist can be calculated as following

$$R_{target} = \begin{bmatrix} i_x & j_x & k_x \\ i_y & j_y & k_y \\ i_z & j_z & k_z \end{bmatrix}$$

$$\theta_6 = \text{atan}2\left(\pm\sqrt{1 - k_y^2}, k_y\right) \quad (2.2.4)$$

$$\theta_7 = \text{atan}2(-j_y, i_y)$$

$$\theta_5 = \text{atan}2(-k_z, k_x)$$

2.2.2 Workspace constraints & Singularity points

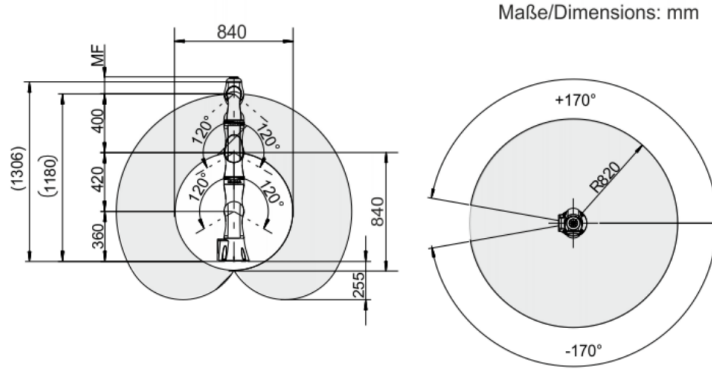


Figure 8: KUKA iiwa LBR14 workspace dimensions

Singularity points:

- When $p_x^2 + p_y^2 = 0$ then the end-effector lies on the z-axis and θ_1 is not defined
- When $\sin(\theta_6) = 0$ then the angles θ_5, θ_7 are not defined

2.2.3 Solutions for 7DoF numerically

Jacobian

$$J = J(\mathbf{q}) = [J_1, J_2, \dots, J_7] \in \mathbb{R}^{6 \times 7}$$

$$J_i = \begin{bmatrix} {}^0\mathbf{z}_i \times ({}^0\mathbf{p}_8 - {}^0\mathbf{p}_i) \\ {}^0\mathbf{z}_i \end{bmatrix} \quad (2.2.5)$$

$J(\mathbf{q})$ is non rectangular and thus non-invertible. Instead of the inverse of the Jacobian the pseudoinverse is calculated which by the equation

$$J^\dagger = J^\top (JJ^\top)^{-1} \quad (2.2.6)$$

2.2.4 Comparison of Inverse Kinematics Techniques

3 Grasping

3.1 Gripper & Forward Kinematics

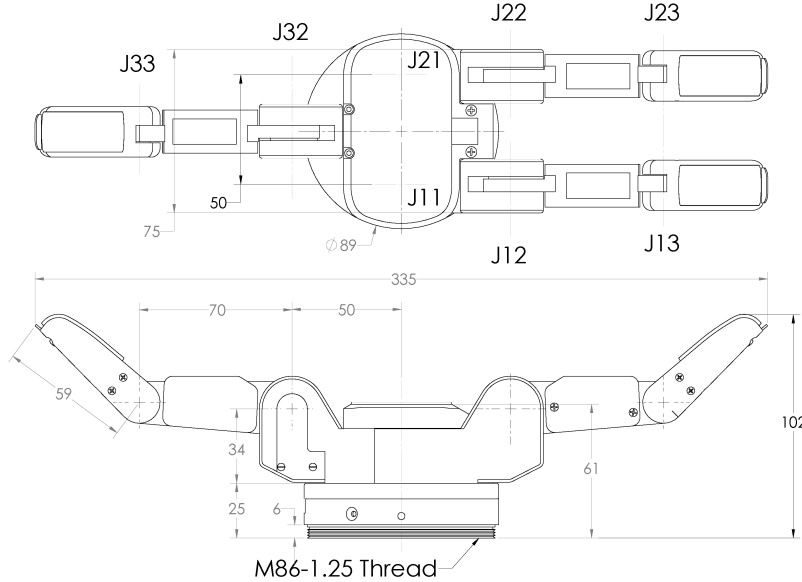


Figure 9: Barrett Hand gripper (model BH8-282) dimensions

3.2 Gripper Inverse Kinematics

The following Inverse Kinematics analysis refers to one finger of the Barrett Hand gripper, which has 3 revolute joints. Finger 3 has only 2 revolute joints for which the angle solutions are the same with the solutions of the last 2 joints of the other fingers. Let

$$\mathbf{p} = \begin{bmatrix} p_x \\ p_y \\ p_z \end{bmatrix}$$

be the position of the grasp point for one finger. The first angle can easily be calculated as

$$\varphi_1 = \text{atan2}(p_y, p_x) \quad (3.2.1)$$

Next, we calculate the third angle based on the law of cosines (see fig.)

$$\begin{aligned} \cos\left(\pi - \varphi_3 - \frac{\pi}{4}\right) &= \frac{L_2^2 + L_3^2 - p^2}{2L_2L_3} \\ \cos\left(\varphi_3 + \frac{\pi}{4}\right) &= \frac{p^2 - L_2^2 - L_3^2}{2L_2L_3} \\ \varphi_3 &= \text{atan2}\left[\pm\sqrt{1 - \left(\frac{p^2 - L_2^2 - L_3^2}{2L_2L_3}\right)^2}, \frac{p^2 - L_2^2 - L_3^2}{2L_2L_3}\right] - \frac{\pi}{4} \end{aligned} \quad (3.2.2)$$

In a more general case, the first argument of the *atan2* function in the expression of φ_3 could also be negative, but in this case this second solution is rejected, because due to mechanical constraints, this angle can't be negative. After having calculated φ_3 we can calculate φ_2

$$\tan(\psi + \varphi_2) = \frac{p_z}{\sqrt{p_x^2 + p_y^2}}$$

$$\tan(\psi) = \frac{L_3 \sin\left(\varphi_3 + \frac{\pi}{4}\right)}{L_2 + L_3 \cos\left(\varphi_3 + \frac{\pi}{4}\right)}$$

$$\varphi_2 = \text{atan}2\left(p_z, \sqrt{p_x^2 + p_y^2}\right) - \text{atan}2\left[L_3 \sin\left(\varphi_3 + \frac{\pi}{4}\right), L_2 + L_3 \cos\left(\varphi_3 + \frac{\pi}{4}\right)\right] \quad (3.2.3)$$

3.3 Force closure

The planar case, the spatial case & convex hull test.

3.4 Firm grasping algorithm & Force control

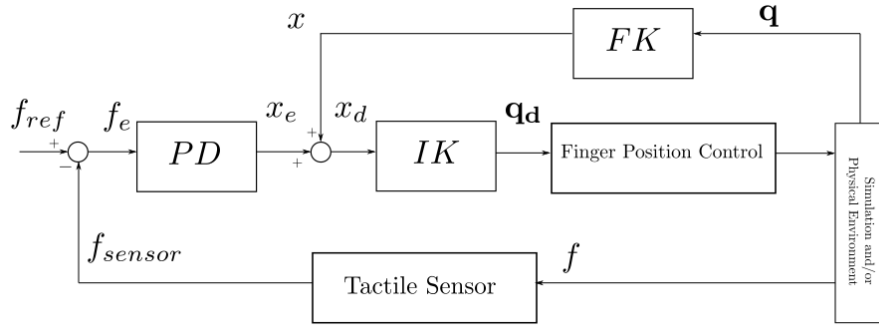


Figure 10: Force control on a Barrett Hand gripper finger

4 Scene and object recognition with Computer Vision

At this section we explore ways to detect and recognize the surgical tools as well as other objects of the simulation scene. To reduce the complexity of this thesis and focus on the more important features of this thesis, we assume in the simulation that the surgical tools are blue and the mounting dock, where the tools will be placed, is green. These assumptions make the scene and object recognition much easier without the need of more advanced image processing and/or machine learning recognition algorithms.

Camera setup used in this thesis:

- 2 HD RGB cameras with resolution 1280×720
- near clipping plane: 0.02
- far clipping plane: 300
- horizontal FoV (field of view): 1.396
- update rate: 30fps

4.1 Laparoscopic tool detection

In order to detect the shape of the tool there are some standard steps that need to be executed. After having loaded the input image we convert it to grayscale, so that we can work on only one channel instead of 3 color channels and thus reduce the amount of calculations. Also for the purposes of extracting the shape of an object, the color doesn't have a very significant role in the algorithm. Next step is to remove the unwanted noise. In this thesis we only assume that the video frames have only Additive White Gaussian Noise (AWGN). To remove some of the noise we use a moving average filter (the filter is also known as a kernel), which is convoluted around the whole image. The filter that was used is the following 3-by-3 matrix

$$h = \frac{1}{9} \begin{bmatrix} 1 & 1 & 1 \\ 1 & 1 & 1 \\ 1 & 1 & 1 \end{bmatrix}$$

the output, filtered image is the result of the convolution of the image with the filter and is calculated as following

$$g(i, j) = \sum_{k,l} f(i + k, j + l)h(k, l)$$

where $g(\cdot, \cdot)$ is the output image and $f(\cdot, \cdot)$ is the input image.

After the noise is removed the image is getting binarized. To do that, we set a threshold, below which the pixels will be black and the rest will be white. This conversion to binary format, makes it easier to extract the boundaries of the black shapes, which will correspond to the boundaries of the objects of the initial image.

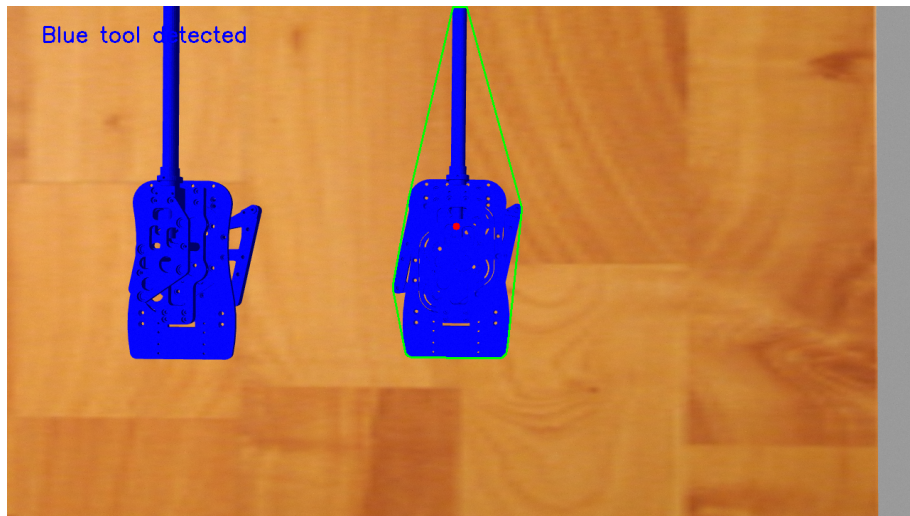


Figure 11: Simple tool detection in simulation based on color, using OpenCV. The green polygon is the convex hull, and the red point is the estimated center of mass

4.2 Stereoscopic vision

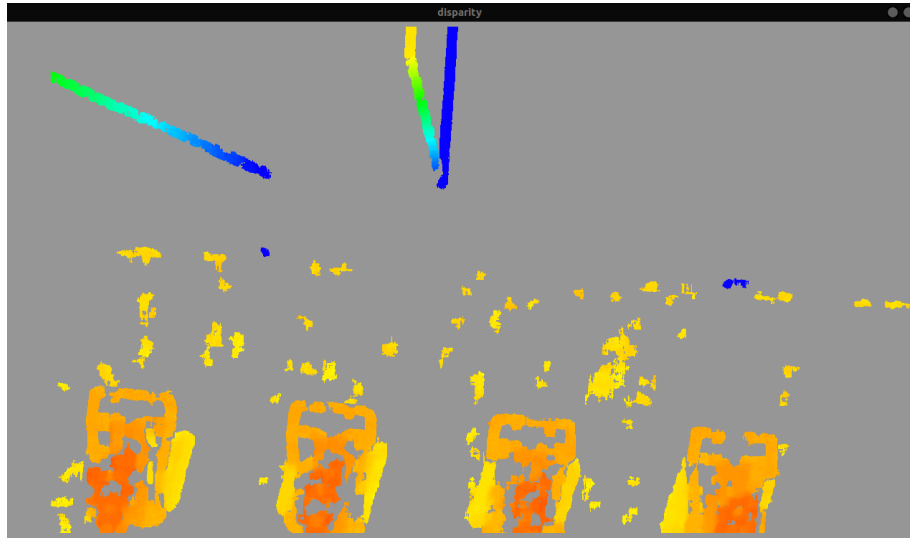


Figure 12: Disparity image calculated from the 2 cameras

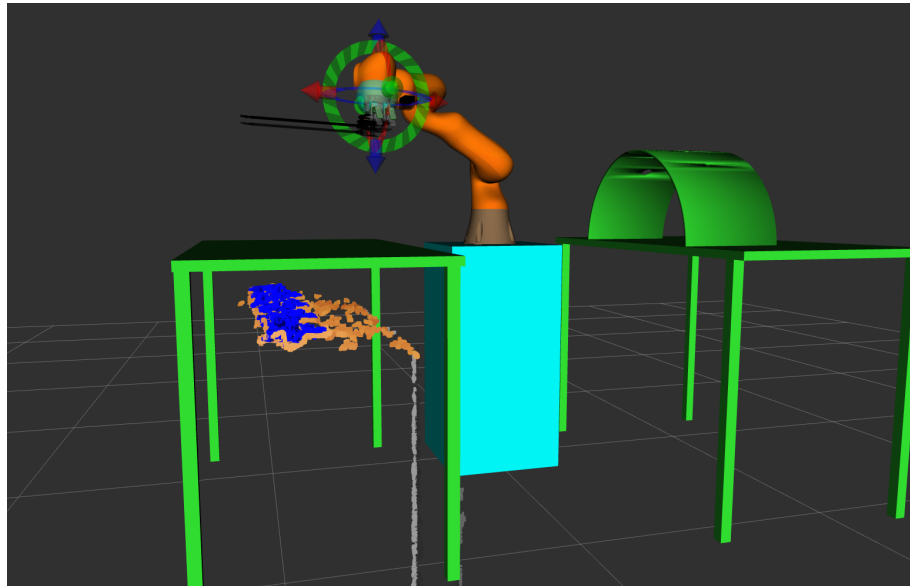


Figure 13: Point cloud of surgical tools, generated from the 2 cameras and visualized in RViz

4.3 Calculation of tool position and orientation

In order for the gripper to grasp correctly the laparoscopic tool, it is required to calculate the tool's position and orientation in the pixel space which must then be converted with respect to the robot's workspace. From all the pixels that have been classified as part of the laparoscopic tool, one can estimate the center of mass and two perpendicular vectors attached to that point that define the orientation. The center of mass is simply the average of the (x, y) coordinates of all the tool's pixels

$$(\bar{x}, \bar{y}) = \left(\frac{1}{N} \sum_{i=1}^N x_i, \frac{1}{N} \sum_{i=1}^N y_i \right)$$

The two orientation vectors are the eigenvectors of the covariance matrix of the above pixels. Let \mathbf{a}, \mathbf{b} be the orientation vectors, then \mathbf{a}, \mathbf{b} are solutions of the equation

$$C\mathbf{v} = \lambda\mathbf{v}$$

where C is the covariance matrix given by

$$C = \begin{bmatrix} \sigma(x, x) & \sigma(x, y) \\ \sigma(y, x) & \sigma(y, y) \end{bmatrix}$$

$$\sigma(x, y) = \frac{1}{n-1} \sum_{i=1}^N (x_i - \bar{x})(y_i - \bar{y})$$

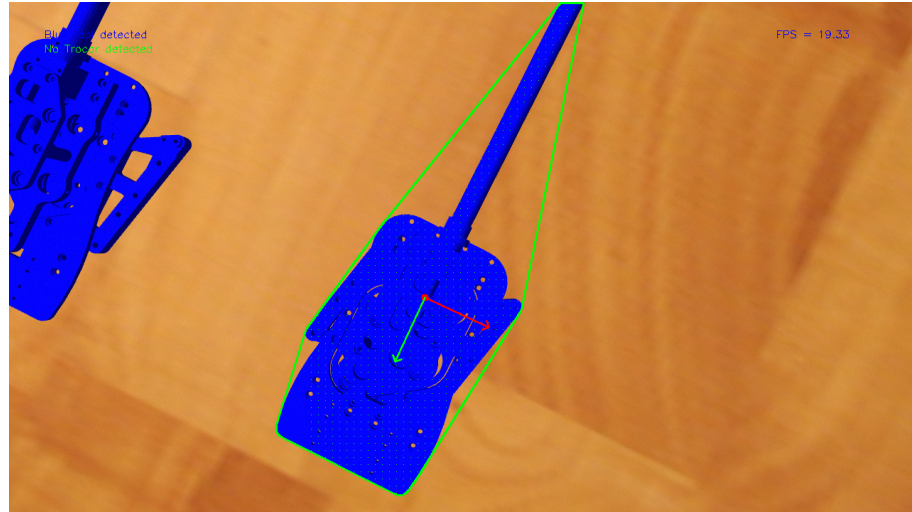


Figure 14: Estimation of tool's pose (position and orientation)

4.4 Calculation of grasping points

4.5 Trocar detection & Estimation of fulcrum point

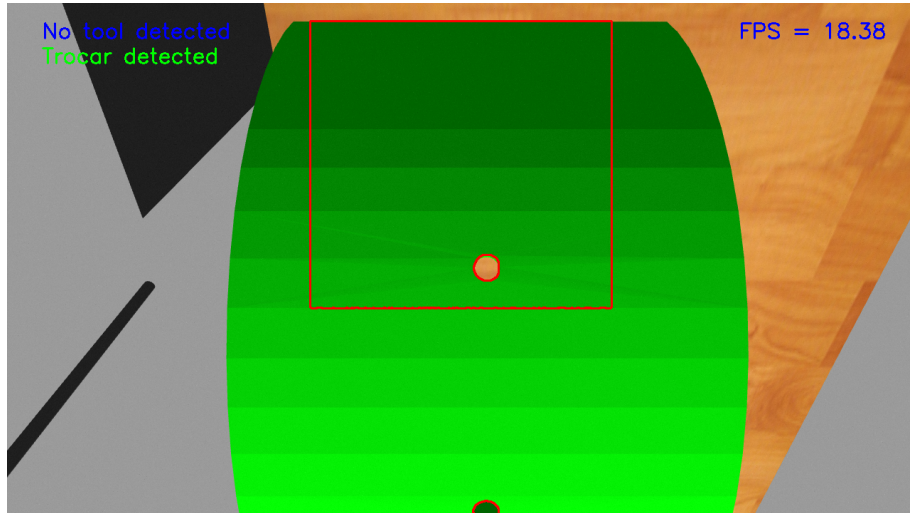


Figure 15: Simple trocar detection in simulation based on color, using OpenCV. In simulation, the trocar is simply considered to be a small cylindrical hole and it's center is the fulcrum point

5 Laparoscopic tool manipulation

The biggest challenge in manipulating a laparoscopic tool with a robot is overcoming the **fulcrum effect** problem. This is also one of the reasons that robotic assisted surgery replaced the traditional laparoscopic procedures. The fulcrum effect means that the surgeon's hand motions are inverted and scaled with respect to the Remote Center of Motion point, which lies approximately on the center of the incision. Apart from the scaling and inversion, laparoscopic procedures add an additional motion constraint that demands at each time one point of the laparoscopic tool to coincide with the RCM point.

5.1 Tool pose

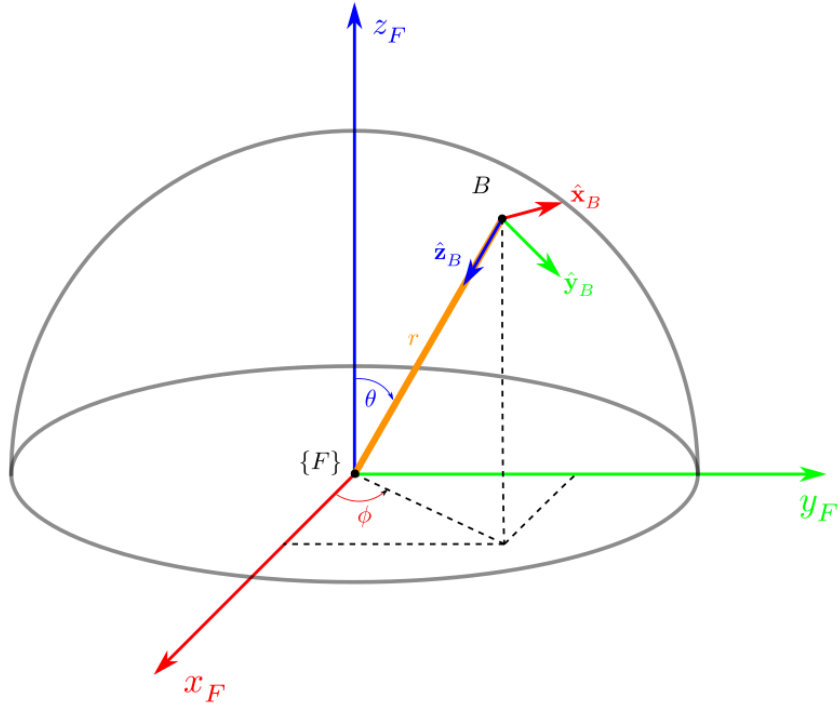


Figure 16: Tool pose at target point B calculated with respect to Fulcrum's reference frame $\{F\}$

The laparoscopic tool pose is given by the position and orientation vectors at target point B with respect to the coordinate frame $\{F\}$. The pose is given by the following transformation matrix

$${}^F T_B = \begin{bmatrix} {}^F R_B & {}^F \mathbf{p}_B \\ \mathbf{0} & 1 \end{bmatrix} \quad \text{where} \quad {}^F R_B = [\hat{\mathbf{x}}_B \quad \hat{\mathbf{y}}_B \quad \hat{\mathbf{z}}_B]$$

$$\hat{\mathbf{x}}_B = \hat{\theta} = \cos(\theta)\cos(\varphi)\hat{\mathbf{x}}_F + \cos(\theta)\sin(\varphi)\hat{\mathbf{y}}_F - \sin(\theta)\hat{\mathbf{z}}_F = \begin{bmatrix} \cos(\theta)\cos(\varphi) \\ \cos(\theta)\sin(\varphi) \\ -\sin(\theta) \end{bmatrix}$$

$$\hat{\mathbf{y}}_B = \hat{\varphi} = -\sin(\varphi)\hat{\mathbf{x}}_F + \cos(\varphi)\hat{\mathbf{y}}_F = \begin{bmatrix} -\sin(\varphi) \\ \cos(\varphi) \\ 0 \end{bmatrix}$$

$$\hat{\mathbf{z}}_B = -\hat{\mathbf{r}} = -(sin(\theta)\cos(\varphi)\hat{\mathbf{x}}_F + sin(\theta)\sin(\varphi)\hat{\mathbf{y}}_F + cos(\theta)\hat{\mathbf{z}}_F) = \begin{bmatrix} -\sin(\theta)\cos(\varphi) \\ -\sin(\theta)\sin(\varphi) \\ -\cos(\theta) \end{bmatrix}$$

The position of the point B is given in spherical coordinates by:

- $r = \rho$: outside penetration of laparoscopic tool
- $\theta = \beta$: altitude angle
- $\varphi = \alpha$: orientation angle

thus the position with respect to the coordinate frame $\{F\}$ is given by

$${}^F \mathbf{p}_B = \begin{bmatrix} \rho \sin(\beta) \cos(\alpha) \\ \rho \sin(\beta) \sin(\alpha) \\ \rho \cos(\beta) \end{bmatrix} = \rho \hat{\mathbf{r}}$$

The above goal point must be the same as the TCP point of the robot's end-effector. This means, that this pose must be converted with respect to the robot's reference frames.

$$\begin{aligned} {}^U T_{TCP} &= {}^U T_B \\ {}^U T_0 {}^0 T_7 {}^7 T_{TCP} &= {}^U T_F {}^F T_B \\ {}^0 T_7 &= {}^U T_0^{-1} {}^U T_F {}^F T_B {}^7 T_{TCP}^{-1} \end{aligned} \quad (5.1.1)$$

5.2 Pivoting motion with respect to Fulcrum Point

On this section, some basic pivoting trajectories around the fulcrum point, are presented. In all of the following three example pivoting motions, we have made the assumption that the position and orientation of the F reference frame is precisely known, which is however not applicable in real-life scenarios ()

5.2.1 Circular trajectory of tool tip

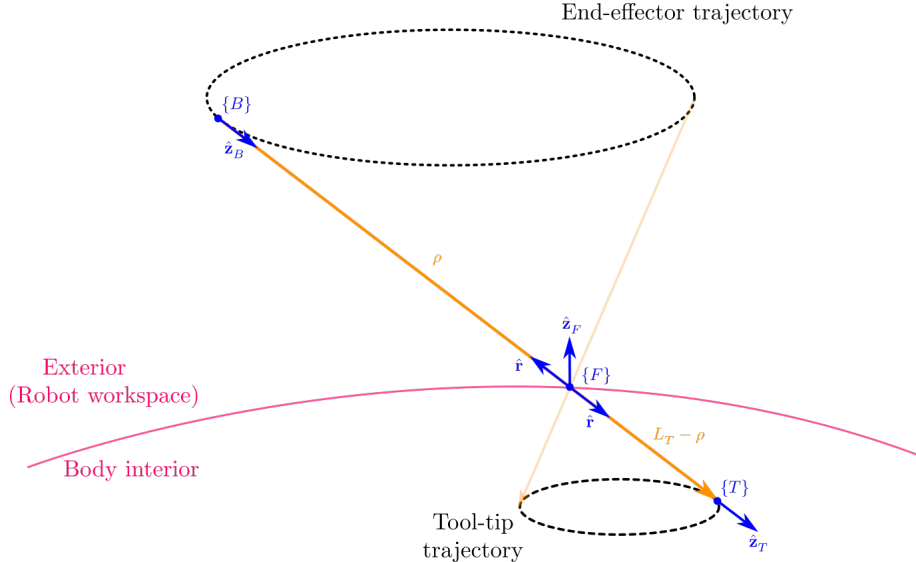


Figure 17: Circular trajectory of tool tip with respect to Fulcrum reference frame

To generate a circular trajectory for the pivot movement we must specify the center of the circle and a vector whose magnitude is the radius of the circle and it's direction gives the orientation of the plane that the circle lies at. The simplest case of a circular trajectory is the one, whose circle lies in a plane parallel to the xy plane.

We first consider the motion of the laparoscopic tool tip on a circle parallel to a z -plane, with respect to the $\{F\}$ coordinate frame.

$$(x_F - x_{F0})^2 + (y_F - y_{F0})^2 = r_0^2, \quad z_F = z_{F0}$$

It's often more convenient to express trajectories in a parametric form, which makes it easier to calculate all the waypoints of the trajectory

$$\begin{cases} x_F = r_0 \cos(2\pi t) + x_{F0} \\ y_F = r_0 \sin(2\pi t) + y_{F0} \\ z_F = z_{F0} \end{cases}, \quad t \in [0, 1]$$

After having calculated the cartesian coordinates we can calculate the spherical coordinates as follows

$$\begin{cases} r = \sqrt{x_F^2 + y_F^2 + z_F^2} \\ \theta = \text{atan2}\left(\sqrt{x_F^2 + y_F^2}, z_F\right) \\ \varphi = \text{atan2}(y_F, x_F) \end{cases} \quad (5.2.1)$$

5.2.2 Circular arc trajectory of tool tip

To generate a circular arc trajectory for a pivot motion we must specify the same parameters as in the circular trajectory as well as the length of the arc or the total angle of the arc section.

5.2.3 Line segment trajectory of tool tip

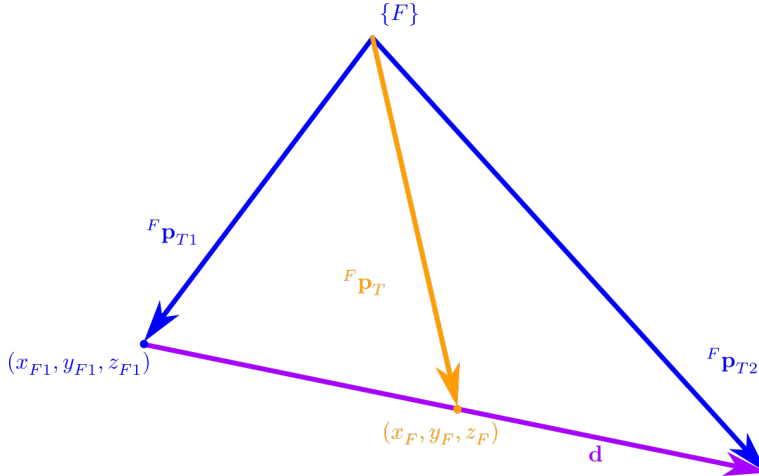


Figure 18: Line segment trajectory of tool tip with respect to Fulcrum reference frame

$$\begin{aligned} \mathbf{d} &= {}^F \mathbf{p}_{T2} - {}^F \mathbf{p}_{T1} = [l, m, n]^\top \\ {}^F \mathbf{p}_T &= [x_F, y_F, z_F]^\top \\ {}^F \mathbf{p}_T &= {}^F \mathbf{p}_{T1} + t \mathbf{d} \\ t &= \frac{x_F - x_{F1}}{l} = \frac{y_F - y_{F1}}{m} = \frac{z_F - z_{F1}}{n} \quad t \in [0, 1] \\ \begin{cases} x_F = tl + x_{F1} = (1-t)x_{F1} + tx_{F2} \\ y_F = tm + y_{F1} = (1-t)y_{F1} + ty_{F2} \\ z_F = tn + z_{F1} = (1-t)z_{F1} + tz_{F2} \end{cases} \end{aligned}$$

After having calculated the cartesian coordinates we can calculate the spherical coordinates using the 5.2.1 equations.

The line segment trajectory of tool tip, as analysed in this section needs no implementation as it is already implemented in the ROS MoveIt library and can be used by calling the method **computeCartesianPath**.

5.3 Task space analysis

Dexterity analysis for tool's task space

$$\mathcal{D} = \mathcal{L}_q \mathcal{M} \quad (5.3.1)$$

where

$$\mathcal{M} = \sqrt{\det(JJ^\top)} \quad (5.3.2)$$

$$\mathcal{L}_q = 1 - \exp \left\{ -\kappa \prod_{i=1}^{n_k} \frac{(q_i - q_{i,\min})(q_{i,\max} - q_i)}{(q_{i,\max} - q_{i,\min})^2} \right\} \quad (5.3.3)$$

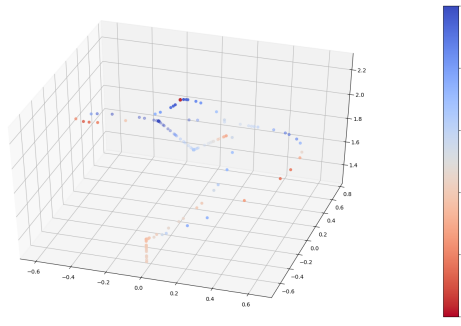


Figure 19: Plot the manipulability of the robot arm at sample points of the executed trajectory

For maximum dexterity at most points of a trajectory in a pivoting motion, the pivot sub- taskspace (i.e. the space of all configurations of feasible pivot motions) must be fully within the robot's whole reachable taskspace, otherwise only a small range of pivot movements will be feasible.

6 Path Planning

6.1 Sampling methods

The path planning algorithms that were mostly used in this thesis belong to the category of sampling methods

6.1.1 RRT Algorithms

The **Rapidly-exploring Random Trees** algorithm is a sampling planning method that searches for an obstacle-free motion plan from an initial state x_{init} to a set of goal states \mathcal{X}_{goal} . We refer to a set of goal states, because apart from the one desired goal state there can be other neighbor states that

are within the allowed position and orientation tolerances.

Algorithm 1: RRT Algorithm

```

foreach replanning attempt do
    initialize vertices  $V \leftarrow \{x_{init}\}$ ;
    initialize edges  $E \leftarrow \emptyset$ ;
    initialize search tree  $T \leftarrow (V, E)$ ;
    while time  $\leq maxPlanningTime$  do
         $x_{rand} \leftarrow \text{getSampleStateFrom}(\mathcal{X})$ ;
         $x_{nearest} \leftarrow \text{getNearestNodeInTreeToState}(T, x_{rand})$ ;
         $x_{new} \leftarrow \text{findLocalPlanFromTo}(x_{nearest}, x_{rand})$ ;
        if  $\text{isPathCollisionFree}(x_{nearest}, x_{rand})$  then
             $V \leftarrow V \cup \{x_{new}\}$ ;
             $E \leftarrow E \cup \{(x_{nearest}, x_{rand})\}$ ;
            if  $x_{new} \in \mathcal{X}_{goal}$  then
                end
            end
        end
    end
end
return FAILURE and  $T = (V, E)$  ;
  
```

Other variations of the RRT Algorithm, which are also available in the OMPL library, included in the MoveIt library of ROS framework are:

- **TRRT** Transition-based RRT
- **BiTRRT** Bidirectional Transition-based RRT
- **RRT***
- **RRTConnect** with is the default OMPL path planner in ROS
- **LBTRRT** Lower Bound Tree RRT

6.1.2 PRM Algorithms

The **Probabilistic Roadmap** (PRM) algorithm is a sampling planning method that constructs a roadmap representation of \mathcal{C}_{free} before searching for a solution. After the roadmap is successfully built, then the algorithm searches for a solution using a traditional graph-based search algorithm. A very important aspect of this algorithm is how the sampling of the free configuration space will be done. The sampling is usually performed using a uniform distribution except from the regions close to

objects where the sampling is more dense.

Algorithm 2: PRM roadmap construction (preprocessing phase)

```

initialize vertices  $V \leftarrow \{x_{init}\}$ ;
initialize edges  $E \leftarrow \emptyset$ ;
initialize roadmap graph  $G \leftarrow (V, E)$ ;
for  $i = 1, \dots, n$  do
     $x_{rand,i} \leftarrow \text{getSampleStateFrom}(\mathcal{X})$ ;
     $\mathcal{N}(x_{rand,i}) \leftarrow \text{getKNearestNeighbors}(G = (V, E), x_{rand,i})$ ;
     $V \leftarrow V \cup \{x_{rand,i}\}$ ;
    foreach  $x \in \mathcal{N}(x_{rand,i})$  do
        if there is no edge between  $x$  and  $x_{rand,i}$  then
            if  $\text{isPathCollisionFree}(x_{nearest}, x_{rand,i})$  then
                 $| E \leftarrow E \cup \{(x_{rand,i}, x), (x, x_{rand,i})\}$ 
            end
        end
    end
end
return  $G = (V, E)$ 

```

Other variations of the PRM Algorithm, which are also available in the OMPL library, included in the MoveIt library of ROS framework are:

- **PRM***
- **LazyPRM**
- **LazyPRM***

6.2 Pick and place algorithm

Algorithm 3: Pick and Place algorithm

```

foreach surgical tool do
    /* Plan the Pick pipeline */  

    set grasp pose;  

    set pre-grasp approach;  

    set post-grasp retreat;  

    set posture of eef before grasp (open gripper);  

    set posture of eef during grasp (closed gripper);  

    /* Plan the Place pipeline */  

    set place location pose;  

    set pre-place approach;  

    set post-grasp retreat;  

    set posture of eef after placing object;  

    Plan pick and place paths;  

end

```

If the pick and place algorithm targets small objects, such as cubes or spheres or other small convex objects then the path planning is straightforward. In the case where, the object to pick and place has at least one dimension that is bigger than the others like a rod or other long objects, such as the surgical tools, used in this thesis, then the path planning becomes more complicated, because of the almost certain collisions of the tool with the links of the rest of the robot (the link of the end-effector will probably not collide with the tool).

7 Trajectory Planning

At this step, given the points of the desired path, a more detailed trajectory is calculated, which will contain all the waypoints that the robot will have to visit.

7.1 Trajectory planning in cartesian coordinates

Connect the points from path planning with line segments and add more points if needed

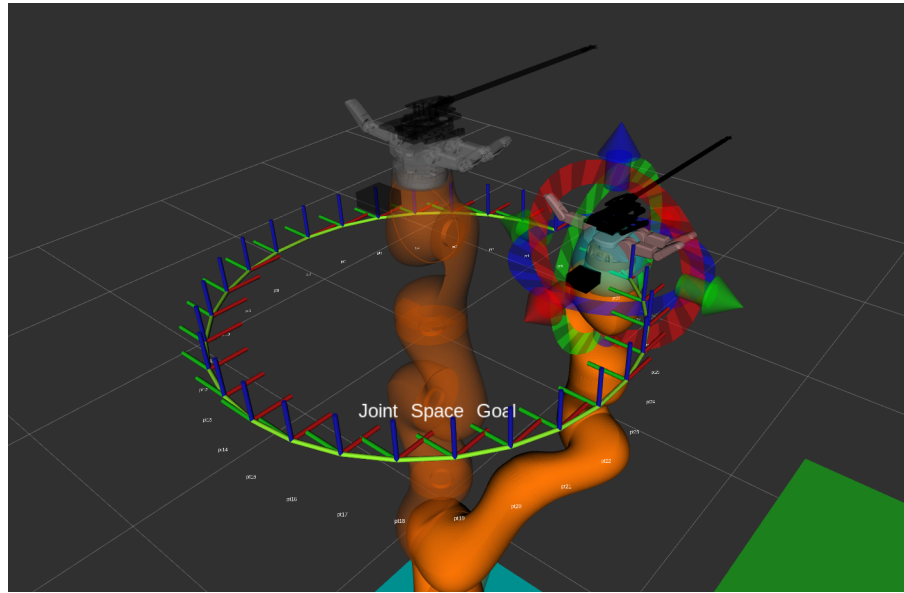


Figure 20: Circular trajectory around the z axis of the home position of the robot

It is very important that the designed trajectory respects the joints angles' range. For example depending on the starting position of the circular trajectory depicted at figure 20, the robot arm may reach it's joint bounds and in order to continue executing the trajectory it will have to make a sudden jump to reset the angles. This could have serious side-effects for both the surgical task and thus the patient, as well as for the operating staff, who control the robot.

7.2 Trajectory planning in joint angles space

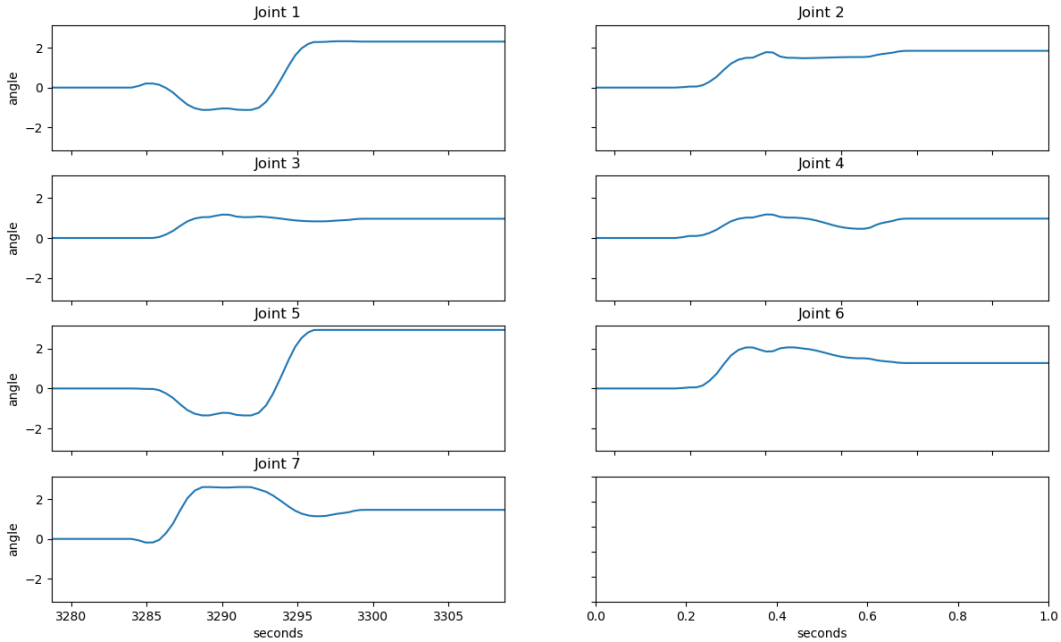


Figure 21: Trajectory diagrams in joints space.

8 Implementation with the ROS framework

8.1 Introduction to the ROS framework

ROS is an open-source robotics software framework. It is a meta-operating system, which means that it provides its own abstractions on top of the host's operating system including filesystem, hardware abstractions, low-level device control, package management and networking. It also provides tools and services to develop large, scalable robotics software, it supports a wide variety of libraries and programming languages and it has a huge community, support and documentation resources.

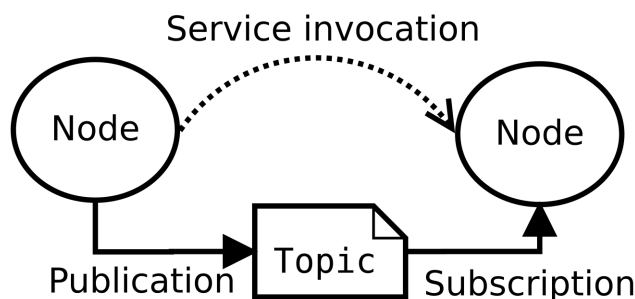


Figure 22: Communication diagram of 2 ROS nodes with a topic and a service

8.2 Gazebo simulation environment

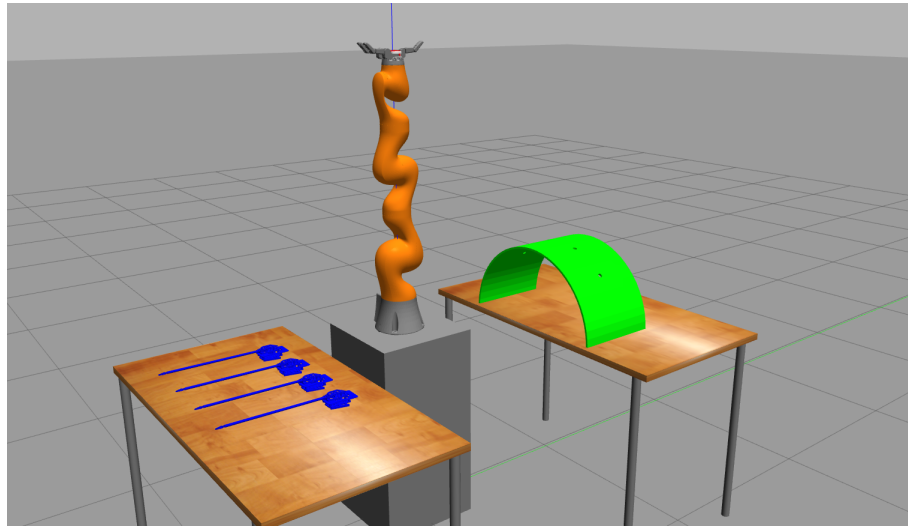


Figure 23: Simulation environment in Gazebo

The main environment setup of this thesis was designed using the Gazebo simulation environment and it consists of the following objects:

- the robot arm, KUKA®iiwa14 lbr, being at the center of the setup
- the robot base, so that the robot arm can better reach the tools and the surgical site and have more flexibility in movement
- 2 tables, one for the tools and one for the surgical site
- 4 surgical tools, using a modified version of the surgical tools used in the Raven II surgical platform
- a mounting dock, which has holes that have the same role as the trocars (small tubes from which the surgical tool is inserted). Initially a mounting dock with 4 same holes of 4mm diameter was used, but it was later replaced with a new one with holes of variable diameters to test feasibility of pivot motions. Larger diameters means more space for motion planner to search for solution and thus more probable to find a solution.

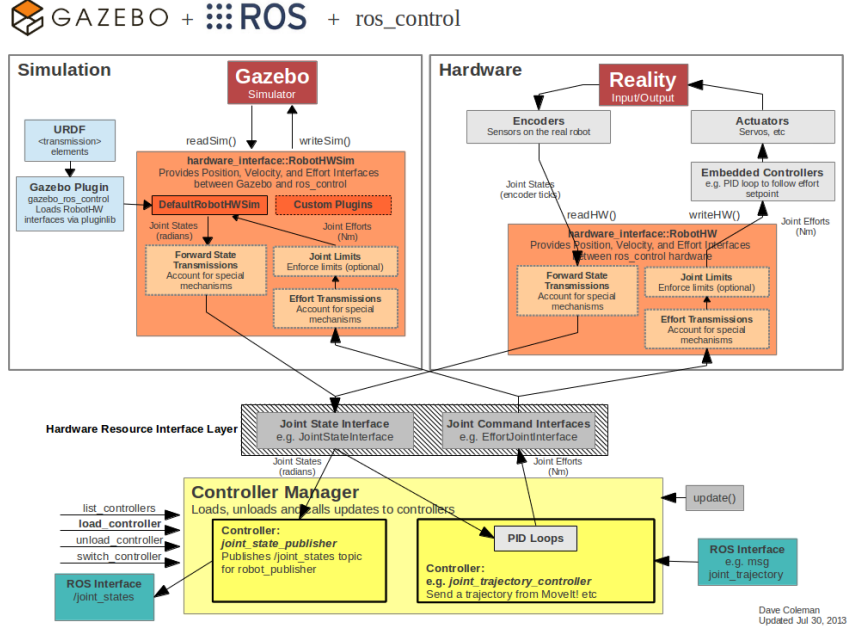


Figure 24: Control & Hardware Interfaces in Gazebo and ROS

8.3 Visualization with RViz

RViz is one of the most important and most used tools in robotic applications development and is a 3D visualizer for the Robot Operating System framework. RViz functionality should not be confused with that of Gazebo, because the first one visualizes the robot state and the **perceived** world (perceived objects or other calculations related to the world) whereas the second one simulates the real world.

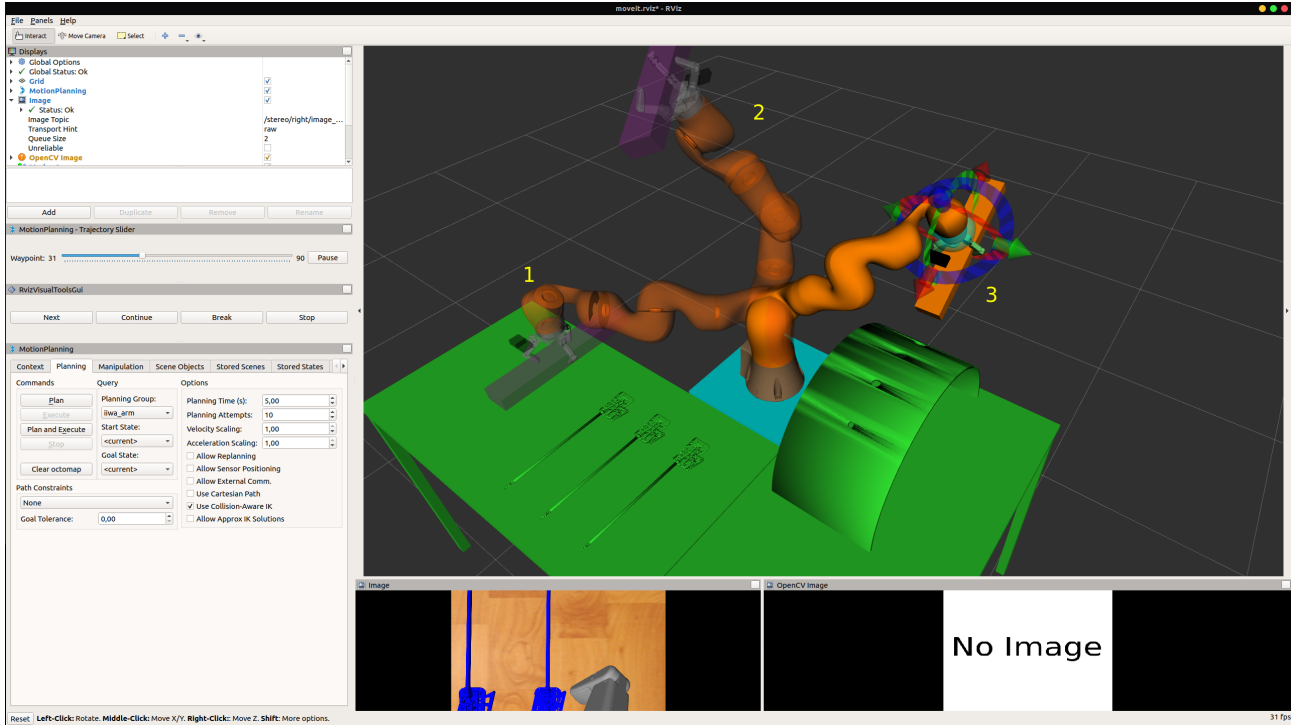


Figure 25: RViz: Visualizing the robot state as well as the state of the perceived world
In this screenshot, various poses of the robot are shown: 1) the current actual real pose of the robot, 2) the planned pose and 3) the goal pose, which can freely be moved within the RViz environment

The objects that appear in RViz can either be visualized from approximations calculated from actual measurements from the robot (for example a point cloud) or can be manually loaded, in which case we make an assumption that the robot already "knows" the exact position, orientation, size and shape of the object, which is rarely the case in real life scenarios. It is important to mention, that every such object is taken into consideration in collision checks and in path planning algorithms.

8.4 Motion Planning with Moveit

Motion Planning parameters outside of body:

- Position tolerance: 50 μ m
- Orientation tolerance: 0.00005 deg
- Planning time: 10s

Motion Planning parameters inside of body:

- Position tolerance:
- Orientation tolerance:
- Planning time
- End-effector interpolation step: 1mm
- Maximum velocity scaling factor

Sometimes the motion planner finds a solution but the execution from the controller is aborted. After many iterations of the same experiment this does not happen always, which means that the feasibility of the execution of the movement by the controller depends on the initial state of the robot, i.e. if

initially some joints of the robot are at their boundaries, then the next commanded trajectory maybe unfeasible.

At each time step it is important to publish a custom message containing all the information about the kinematic state of the robot. In this thesis a custom **ROS** message was created containing a tf transform with a 3D vector for the position and a quaternion for the rotation and a custom 6-by-7 matrix containing the values of the Jacobian. The MoveIt library, from which the kinematic state of the robot is obtained, returns the orientation of the end effector as a 3-by-3 rotation matrix, but in the ROS tf message it must be expressed as a quaternion. To convert the matrix to a quaternion we first calculate the euler angles and then use these values to construct the quaternion “vector”. The quaternion representation of rotation is often preferred in robotic applications due to its efficiency in calculations and memory. To convert the transformation matrix to euler angles and then to quaternions the following formulas were used:

$$T = \begin{bmatrix} r_{11} & r_{12} & r_{13} & x \\ r_{21} & r_{22} & r_{23} & y \\ r_{31} & r_{32} & r_{33} & z \\ 0 & 0 & 0 & 1 \end{bmatrix}$$

$$\varphi = \text{atan2}(r_{21}, r_{11})$$

$$\theta = \text{atan2}(-r_{31}, \sqrt{r_{11}^2 + r_{21}^2})$$

$$\psi = \text{atan2}(r_{32}, r_{33})$$

where T is the transformation matrix and φ, θ, ψ are the roll, pitch and yaw (Euler) angles.

8.5 Experiments and Development methodology

8.5.1 Robot Planner 1

In this first experiment we are testing some simple trajectories with the surgical tool already attached to the robot arm’s end effector. The path is designed using the appropriate coordinates and orientations so that the robot begins from the home position, then visits the table with the surgical tools and then visits the other table on top of which the mounting dock is placed. Upon arrival at the mounting dock, the robot inserts the tool inside a hole (we consider these holes to be a simplistic alternative to the trocars used in real operations), then executes a simple pivot motion, while the tool is still inserted and then the tool gets ejected from the mounting dock’s hole.

The aim of this experiment is to test the overall behaviour of the robot inside the work space, before implementing more complex path planning algorithms.

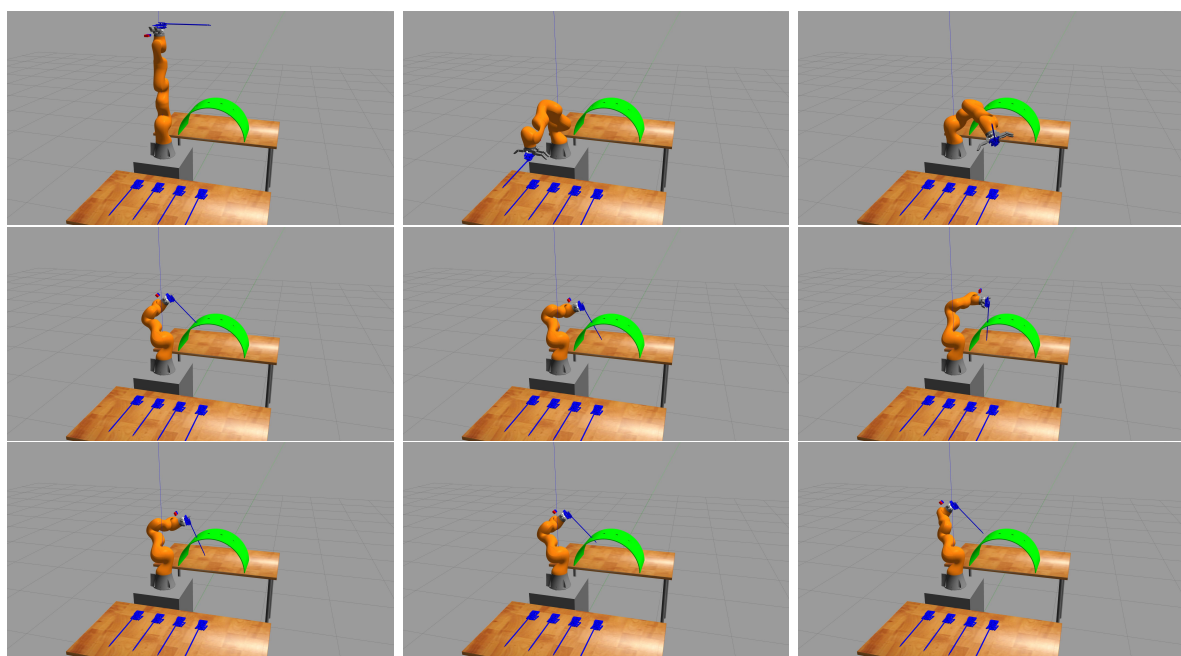


Figure 26: Experiment 1:

8.5.2 Robot Planner 2

In this experiment, we plan a path such that the robot arm will visit all holes of the mounting dock and will try the insertion movement of the surgical tool. This experiment is very useful, because it shows whether all holes of the mounting dock are **reachable** (inside the robot's work space) and if so, how **dexterous** the robot will be in pivoting around each hole, i.e. how free the robot arm is to execute pivot motions.

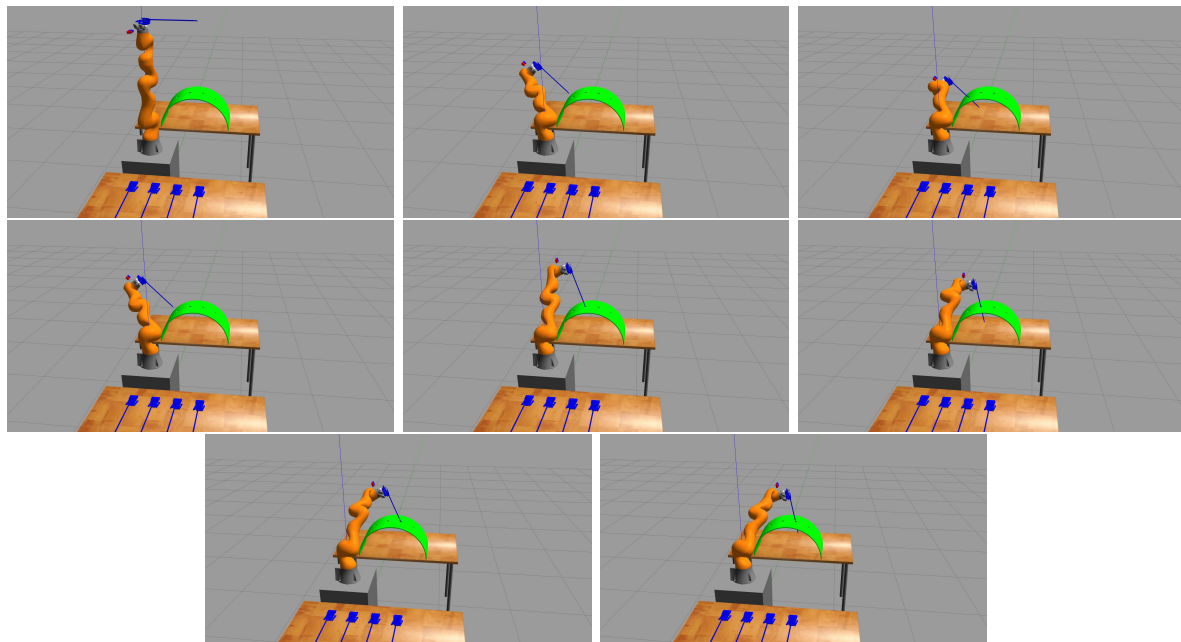


Figure 27: Experiment 2a:

To overcome the reachability issue shown in Figure 27, the algorithm was repeated, but this time using a different simulation layout in Gazebo, in which the mounting dock is closer to the robot and in front of it. This new layout enables the robot to reach all mounting holes with ease and with sufficient dexterity, the robot is free to pivot around.

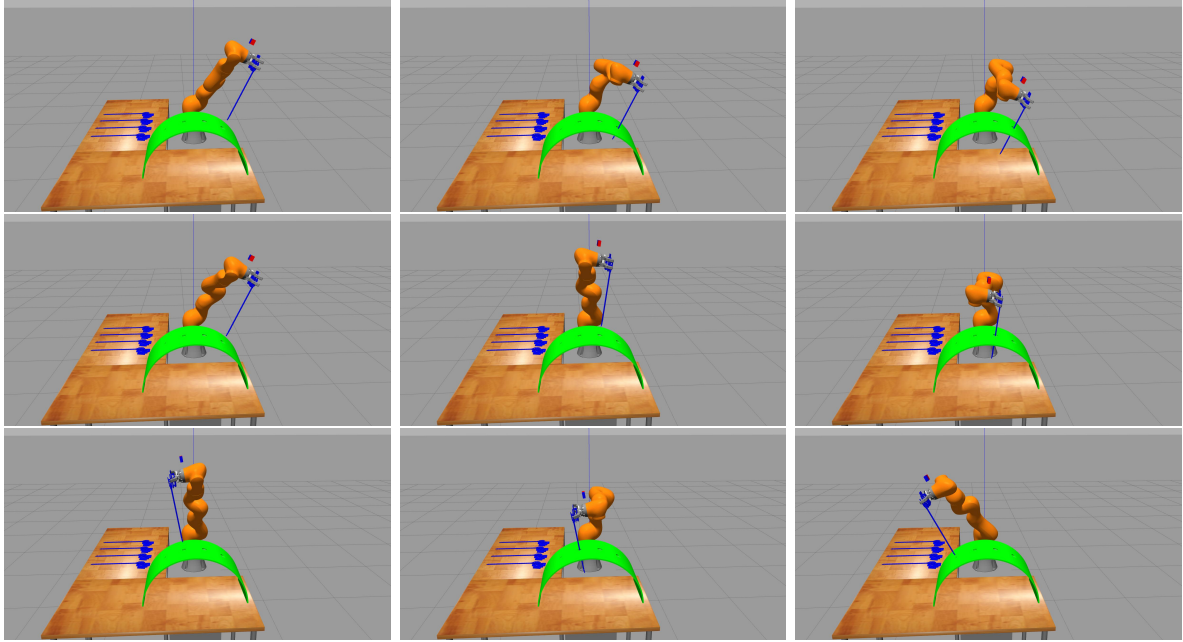


Figure 28: Experiment 2b:

Due to the probabilistic nature of the motion planner (in these experiments the OMPL library is used with the RRTConnect path planning algorithm), the solutions to the path planning problem are not always the same and thus it is possible that the robot arm reaches a pose which is close to a singularity

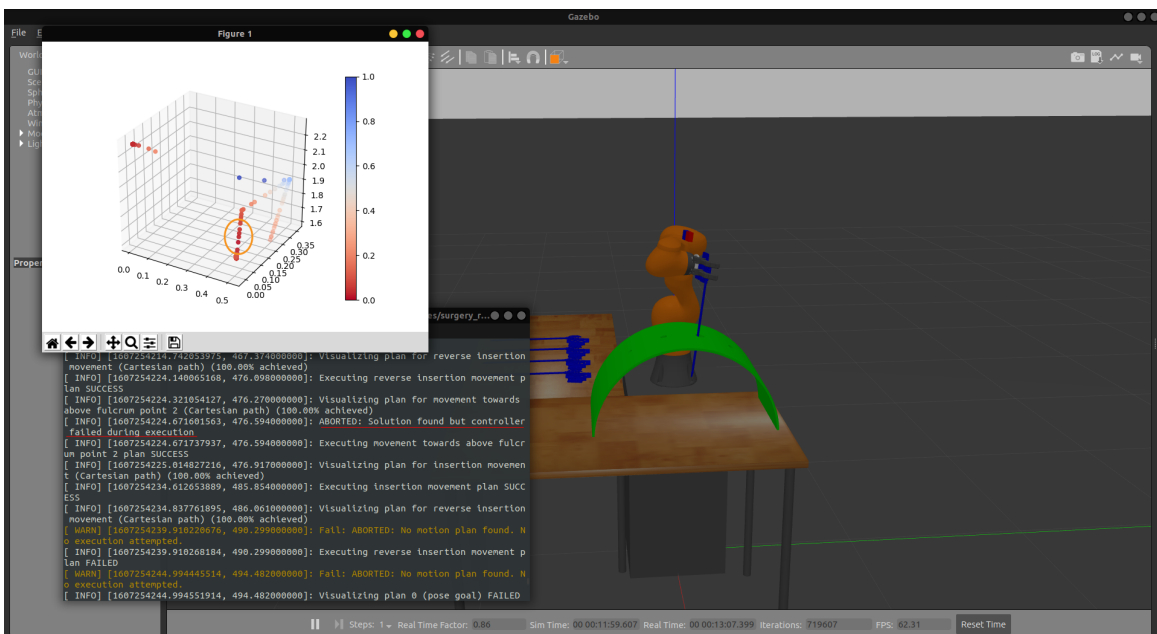


Figure 29: Experiment 2b: Singularity failure

		RRTConnect							
Robot Planner 4		Pick Pipeline				Place Pipeline			
Experiment	Status	Solution Time	Path Simplification Time	Planning Attempts	Status	Solution Time	Path Simplification Time	Planning Attempts	
1	1	0.026189	0.065173	1	1	0.014644	0.020947	1	
2									
3									
4									
5									
Average									

8.5.3 Robot Planner 3

8.5.4 Robot Planner 4

8.5.5 Robot Planner 5

9 Results and Future Work

9.1 Results

9.2 Conclusions & Comparison with similar projects

9.3 Future Work

Appendices

A Software and Documentation

- All software that developed for this thesis is available and will be maintained at https://github.com/karadalex/surgery_robotics_kuka_barrett
- Instruction on how to run the software of this thesis, as well as documentation of the various software components is available and will be maintained at https://karadalex.github.io/surgery_robotics_kuka_barrett/

B Mathematics

B.1 Euler angles to Quaternions

Let θ, ϕ, ψ be the Euler angles (roll, pitch, yaw) respectively, then using the following equations

$$c\theta = \cos\left(\frac{\theta}{2}\right), s\theta = \sin\left(\frac{\theta}{2}\right)$$

$$c\varphi = \cos\left(\frac{\varphi}{2}\right), s\varphi = \sin\left(\frac{\varphi}{2}\right)$$

$$c\psi = \cos\left(\frac{\psi}{2}\right), s\psi = \sin\left(\frac{\psi}{2}\right)$$

we can calculate the associated quaternion, in vector notation, as follows

$$\mathbf{q} = \begin{bmatrix} q_x \\ q_y \\ q_z \\ q_w \end{bmatrix} = \begin{bmatrix} s\theta c\varphi c\psi - c\theta s\varphi s\psi \\ c\theta s\varphi c\psi + s\theta c\varphi s\psi \\ c\theta c\varphi s\psi - s\theta s\varphi c\psi \\ c\theta c\varphi c\psi + s\theta s\varphi s\psi \end{bmatrix}$$

Nomenclature

$\hat{\mathbf{r}}, \hat{\boldsymbol{\theta}}, \hat{\boldsymbol{\phi}}$ Unit vectors of r, θ, φ axes respectively, in spherical coordinates

$\hat{\mathbf{x}}, \hat{\mathbf{y}}, \hat{\mathbf{z}}$ Unit vectors of x, y, z axes respectively

\mathcal{C} Configuration Space

\mathcal{C}_{free} Free Configuration Space

\mathcal{C}_{obs} Obstacle Space

\mathcal{L}_q Dexterity measure of the robotic arm

\mathcal{M} Manipulability measure of the robotic arm

θ, ϕ, ψ roll, pitch, yaw angles, also known as the Euler angles

${}^{i-1}\mathbf{p}_{iO}$ Position vector from the origin of the coordinate frame $\{i\}$ to the origin of the coordinate frame $\{i - 1\}$

${}^{i-1}R_i$ Rotation matrix from coordinate frame $\{i\}$ to coordinate frame $\{i - 1\}$

${}^{i-1}T_i$ Transformation matrix from coordinate frame $\{i\}$ to coordinate frame $\{i - 1\}$

c_i Shorthand notation for $\cos\theta_i$

J^\dagger Pseudoinverse of the Jacobian

s_i Shorthand notation for $\sin\theta_i$

List of Figures

1	The PUMA 560 robotic arm, which was the first to be used in surgery robotics in 1985	10
2	DaVinci Xi, ©2020 Intuitive Surgical, Inc. Patient Cart with the robotic arms that control the surgical tools	11
3	The Monarch™ Platform endoscopic system	12
4	DaVinci Xi ©2020 Intuitive Surgical, Inc. Surgeon Console	13
5	Kanban view of backlog tasks to organize all features, requirements and tasks needed to complete this thesis. The tool used to keep track of all tasks is Airtable	14
6	Joint reference frames of the KUKA iiwa14 robot	15
7	Calculation of angles θ_2, θ_4	16
8	KUKA iiwa LBR14 workspace dimensions	17
9	Barrett Hand gripper (model BH8-282) dimensions	18
10	Force control on a Barrett Hand gripper finger	19
11	Simple tool detection in simulation based on color, using OpenCV. The green polygon is the convex hull, and the red point is the estimated center of mass	20
12	Disparity image calculated from the 2 cameras	21
13	Point cloud of surgical tools, generated from the 2 cameras and visualized in RViz	21
14	Estimation of tool's pose (position and orientation)	22
15	Simple trocar detection in simulation based on color, using OpenCV. In simulation, the trocar is simply considered to be a small cylindrical hole and it's center is the fulcrum point	22
16	Tool pose at target point B calculated with respect to Fulcrum's reference frame $\{F\}$.	23
17	Circular trajectory of tool tip with respect to Fulcrum reference frame	24
18	Line segment trajectory of tool tip with respect to Fulcrum reference frame	25
19	Plot the manipulability of the robot arm at sample points of the executed trajectory .	26
20	Circular trajectory around the z axis of the home position of the robot	29
21	Trajectory diagrams in joints space	30
22	Communication diagram of 2 ROS nodes with a topic and a service	30
23	Simulation environment in Gazebo	31
24	Control & Hardware Interfaces in Gazebo and ROS	32
25	RViz: Visualizing the robot state as well as the state of the perceived world. In this screenshot, various poses of the robot are shown: 1) the current actual real pose of the robot, 2) the planned pose and 3) the goal pose, which can freely be moved within the RViz environment	33
26	Experiment 1:	35
27	Experiment 2a:	35
28	Experiment 2b:	36
29	Experiment 2b: Singularity failure	36

List of Algorithms

1	RRT Algorithm	27
2	PRM roadmap construction (preprocessing phase)	28
3	Pick and Place algorithm	28

Bibliography

- [1] Nastaran Aghakhani et al. "Task control with remote center of motion constraint for minimally invasive robotic surgery". In: *2013 IEEE International Conference on Robotics and Automation* (2013), pp. 5807–5812.
- [2] E. Bauzano et al. "Active wrists endoscope navigation in robotized laparoscopic surgery". In: *2009 IEEE International Conference on Mechatronics*. Apr. 2009, pp. 1–6. DOI: 10.1109/ICMECH.2009.4957177.
- [3] E. Boctor et al. "Virtual Remote Center of Motion Control for Needle Placement Robots". In: *Computer aided surgery : official journal of the International Society for Computer Aided Surgery* 9 5 (2003), pp. 175–83.
- [4] M. C. Capolei et al. "Positioning the laparoscopic camera with industrial robot arm". In: *2017 3rd International Conference on Control, Automation and Robotics (ICCAR)*. Apr. 2017, pp. 138–143. DOI: 10.1109/ICCAR.2017.7942675.
- [5] Sachin Chitta et al. "ros_control: A generic and simple control framework for ROS". In: *The Journal of Open Source Software* (2017). DOI: 10.21105/joss.00456. URL: <http://www.theoj.org/joss-papers/joss.00456/10.21105.joss.00456.pdf>.
- [6] G. Cowley. "Introducing "Robodoc". A robot finds his calling—in the operating room". In: *Newsweek* 120.21 (Nov. 1992), p. 86.
- [7] Bassem Dahroug, B. Tamadazte, and N. Andreff. "3D Path Following with Remote Center of Motion Constraints". In: *ICINCO*. 2016.
- [8] Bassem Dahroug, B. Tamadazte, and N. Andreff. "Task Controller for Performing Remote Centre of Motion". In: *ICINCO*. 2016.
- [9] Bassem Dahroug, B. Tamadazte, and N. Andreff. "Visual servoing controller for time-invariant 3D path following with remote centre of motion constraint". In: *2017 IEEE International Conference on Robotics and Automation (ICRA)* (2017), pp. 3612–3618.
- [10] Bassem Dahroug, Brahim Tamadazte, and Nicolas Andreff. "Unilaterally Constrained Motion of a Curved Surgical Tool". In: *Robotica* (2020), pp. 1–23. DOI: 10.1017/S0263574719001735.
- [11] M. M. Dalvand and B. Shirinzadeh. "Remote centre-of-motion control algorithms of 6-RRCRR parallel robot assisted surgery system (PRAMiSS)". In: *2012 IEEE International Conference on Robotics and Automation* (2012), pp. 3401–3406.
- [12] Carlos Faria et al. "Position-based kinematics for 7-DoF serial manipulators with global configuration control, joint limit and singularity avoidance". In: *Mechanism and Machine Theory* 121 (2018), pp. 317–334. ISSN: 0094-114X. DOI: <https://doi.org/10.1016/j.mechmachtheory.2017.10.025>. URL: <http://www.sciencedirect.com/science/article/pii/S0094114X17306559>.
- [13] Tully Foote. "tf: The transform library". In: *Technologies for Practical Robot Applications (TePRA), 2013 IEEE International Conference on*. Open-Source Software workshop. Apr. 2013, pp. 1–6. DOI: 10.1109/TePRA.2013.6556373.
- [14] K. Fujii et al. "Gaze contingent cartesian control of a robotic arm for laparoscopic surgery". In: *2013 IEEE/RSJ International Conference on Intelligent Robots and Systems*. Nov. 2013, pp. 3582–3589. DOI: 10.1109/IROS.2013.6696867.
- [15] M. Fujii et al. "Relationship between workspace reduction due to collisions and distance between endoscope and target organ in pediatric endoscopic surgery". In: *5th IEEE RAS/EMBS International Conference on Biomedical Robotics and Biomechatronics*. Aug. 2014, pp. 46–51. DOI: 10.1109/BIOROB.2014.6913750.
- [16] J. Funda et al. "Constrained Cartesian motion control for teleoperated surgical robots". In: *IEEE Trans. Robotics Autom.* 12 (1996), pp. 453–465.

- [17] J. Funda et al. "Control and evaluation of a 7-axis surgical robot for laparoscopy". In: *Proceedings of 1995 IEEE International Conference on Robotics and Automation*. Vol. 2. 1995, 1477–1484 vol.2.
- [18] Alessandro Gasparetto et al. "Path Planning and Trajectory Planning Algorithms: A General Overview". In: *Motion and Operation Planning of Robotic Systems: Background and Practical Approaches*. Ed. by Giuseppe Carbone and Fernando Gomez-Bravo. Cham: Springer International Publishing, 2015, pp. 3–27. ISBN: 978-3-319-14705-5. DOI: 10.1007/978-3-319-14705-5_1. URL: https://doi.org/10.1007/978-3-319-14705-5_1.
- [19] G. Gras et al. "Implicit gaze-assisted adaptive motion scaling for highly articulated instrument manipulation". In: *2017 IEEE International Conference on Robotics and Automation (ICRA)*. May 2017, pp. 4233–4239. DOI: 10.1109/ICRA.2017.7989488.
- [20] Techbriefs Media Group. *Surgical Robotics: The Evolution of a Medical Technology - Medical Design Briefs*. URL: <https://www.medicaldesignbriefs.com/component/content/article/mdb/features/technology-leaders/25006> (visited on 09/18/2020).
- [21] G. B. Hanna, S. Shimi, and A. Cuschieri. "Optimal port locations for endoscopic intracorporeal knotting". In: *Surgical Endoscop* 11.4 (Apr. 1997), pp. 397–401. ISSN: 1432-2218. DOI: 10.1007/s004649900374. URL: <https://doi.org/10.1007/s004649900374>.
- [22] B. Hannaford et al. "Raven-II: An Open Platform for Surgical Robotics Research". In: *IEEE Transactions on Biomedical Engineering* 60.4 (Apr. 2013), pp. 954–959. ISSN: 1558-2531. DOI: 10.1109/TBME.2012.2228858.
- [23] M. R. Hasan et al. "Modelling and Control of the Barrett Hand for Grasping". In: *2013 UKSim 15th International Conference on Computer Modelling and Simulation*. Apr. 2013, pp. 230–235. DOI: 10.1109/UKSim.2013.142.
- [24] Felix C. Huang et al. "Learning kinematic mappings in laparoscopic surgery". In: *Conference proceedings : ... Annual International Conference of the IEEE Engineering in Medicine and Biology Society. IEEE Engineering in Medicine and Biology Society. Annual Conference 2010* (2010). PMC3280950[pmcid], pp. 2097–2102. ISSN: 1557-170X. DOI: 10.1109/IEMBS.2010.5626188. URL: <https://pubmed.ncbi.nlm.nih.gov/21095685>.
- [25] J. Hutzl and H. Wörn. "Spatial probability distribution for port planning in minimal invasive robotic surgery (MIRS)". In: *2015 6th International Conference on Automation, Robotics and Applications (ICARA)*. Feb. 2015, pp. 204–210. DOI: 10.1109/ICARA.2015.7081148.
- [26] Reza N. Jazar. *Theory of Applied Robotics, Kinematics, Dynamics, and Control (2nd Edition)*. Springer, Boston, MA, 2010. ISBN: 978-1-4419-1750-8. DOI: 10.1007/978-1-4419-1750-8.
- [27] S. Karaman and Emilio Frazzoli. "Sampling-based algorithms for optimal motion planning". In: *The International Journal of Robotics Research* 30 (2011), pp. 846–894.
- [28] Abbas Karami et al. "Force, orientation and position control in redundant manipulators in prioritized scheme with null space compliance". In: *Control Engineering Practice* 85 (2019), pp. 23–33.
- [29] J. J. Kuffner and S. M. LaValle. "RRT-connect: An efficient approach to single-query path planning". In: *Proceedings 2000 ICRA. Millennium Conference. IEEE International Conference on Robotics and Automation. Symposia Proceedings (Cat. No.00CH37065)*. Vol. 2. Apr. 2000, 995–1001 vol.2. DOI: 10.1109/ROBOT.2000.844730.
- [30] I. Kuhlemann et al. "Robust inverse kinematics by configuration control for redundant manipulators with seven DoF". In: *2016 2nd International Conference on Control, Automation and Robotics (ICCAR)*. Apr. 2016, pp. 49–55. DOI: 10.1109/ICCAR.2016.7486697.
- [31] P. Lago, Carlo Lombardi, and I. Vallone. "From laparoscopic surgery to 3-D double console robot-assisted surgery". In: *Proceedings of the 10th IEEE International Conference on Information Technology and Applications in Biomedicine* (2010), pp. 1–4.

- [32] Kevin M Lynch and Frank C. Park. *Modern Robotics: Mechanics, Planning, and Control*. English (US). Cambridge Univeristy Press, 2017. ISBN: 978-1107156302.
- [33] M. Marinho et al. “A Unified Framework for the Teleoperation of Surgical Robots in Constrained Workspaces”. In: *2019 International Conference on Robotics and Automation (ICRA)* (2019), pp. 2721–2727.
- [34] Murilo M. Marinho, Mariana C. Bernardes, and Antônio Padilha Lanari Bo. “A programmable remote center-of-motion controller for minimally invasive surgery using the dual quaternion framework”. In: *5th IEEE RAS/EMBS International Conference on Biomedical Robotics and Biomechatronics* (2014), pp. 339–344.
- [35] Q. Mei et al. “PROBOT — A computer integrated prostatectomy system”. In: *Visualization in Biomedical Computing*. Ed. by Karl Heinz Höhne and Ron Kikinis. Berlin, Heidelberg: Springer Berlin Heidelberg, 1996, pp. 581–590. ISBN: 978-3-540-70739-4.
- [36] Victor F. Muñoz et al. “Pivoting motion control for a laparoscopic assistant robot and human clinical trials”. In: *Advanced Robotics* 19 (2005), pp. 694–712.
- [37] A. A. Navarro et al. “Automatic positioning of surgical instruments in minimally invasive robotic surgery through vision-based motion analysis”. In: *2007 IEEE/RSJ International Conference on Intelligent Robots and Systems*. Oct. 2007, pp. 202–207. DOI: 10.1109/IROS.2007.4399150.
- [38] Jason M. O’Kane. *A Gentle Introduction to ROS*. Available at <http://www.cse.sc.edu/~jokane/agitr/>. Independently published, Oct. 2013. ISBN: 978-1492143239.
- [39] Claudio Pacchierotti. “Needle Insertion in Simulated Soft Tissue”. In: *Cutaneous Haptic Feedback in Robotic Teleoperation*. Cham: Springer International Publishing, 2015, pp. 21–36. ISBN: 978-3-319-25457-9. DOI: 10.1007/978-3-319-25457-9_2. URL: https://doi.org/10.1007/978-3-319-25457-9_2.
- [40] Jaydeep Palep. “Robotic assisted minimally invasive surgery”. In: *Journal of minimal access surgery* 5 (Feb. 2009), pp. 1–7. DOI: 10.4103/0972-9941.51313.
- [41] C. Pham et al. “Analysis of a moving remote center of motion for robotics-assisted minimally invasive surgery”. In: *2015 IEEE/RSJ International Conference on Intelligent Robots and Systems (IROS)* (2015), pp. 1440–1446.
- [42] Morgan Quigley et al. “ROS: an open-source Robot Operating System”. In: *ICRA Workshop on Open Source Software*. 2009.
- [43] S. Roh et al. “Development of the SAIT single-port surgical access robot slave arm based on RCM Mechanism”. In: *2015 37th Annual International Conference of the IEEE Engineering in Medicine and Biology Society (EMBC)* (2015), pp. 5285–5290.
- [44] *ROS/Concepts - ROS Wiki*. URL: <https://wiki.ros.org/ROS/Concepts> (visited on 09/19/2020).
- [45] Benoît Rosa et al. “Estimation of optimal pivot point for remote center of motion alignment in surgery”. In: *International Journal of Computer Assisted Radiology and Surgery* 10.2 (Feb. 2015), pp. 205–215. ISSN: 1861-6429. DOI: 10.1007/s11548-014-1071-3. URL: <https://doi.org/10.1007/s11548-014-1071-3>.
- [46] Hamid Sadeghian, Fatemeh Zokaei, and Shahram Hadian Jazi. “Constrained Kinematic Control in Minimally Invasive Robotic Surgery Subject to Remote Center of Motion Constraint”. In: *Journal of Intelligent & Robotic Systems* (2019), pp. 1–13.
- [47] H. Shao et al. “A New CT-Aided Robotic Stereotaxis System”. In: 1985.
- [48] I. A. Şucan and S. Chitta. *Moveit!* URL: <https://moveit.ros.org/> (visited on 04/28/2020).
- [49] V. Vitiello et al. “Emerging Robotic Platforms for Minimally Invasive Surgery”. In: *IEEE Reviews in Biomedical Engineering* 6 (2013), pp. 111–126.
- [50] Go Watanabe, ed. *Robotic Surgery*. Springer Japan, 2014. DOI: 10.1007/978-4-431-54853-9. URL: <https://doi.org/10.1007/978-4-431-54853-9>.

- [51] Haiwang Xu et al. "Laparoscopic Robot Design and Kinematic Validation". In: Jan. 2007, pp. 1426–1431. doi: 10.1109/ROBIO.2006.340138.
- [52] Tao Yang et al. "Mechanism of a Learning Robot Manipulator for Laparoscopic Surgical Training". In: *Intelligent Autonomous Systems 12*. Ed. by Sukhan Lee et al. Berlin, Heidelberg: Springer Berlin Heidelberg, 2013, pp. 17–26. ISBN: 978-3-642-33932-5.
- [53] L. Yu et al. "Research on the Trajectory Planning of the Minimally Invasive Surgical Robot 6-DOF Manipulator". In: *2010 International Conference on Biomedical Engineering and Computer Science*. Apr. 2010, pp. 1–4. doi: 10.1109/ICBECS.2010.5462451.
- [54] Xiaoqin Zhou et al. "New remote centre of motion mechanism for robot-assisted minimally invasive surgery". In: *BioMedical Engineering OnLine* 17 (2018).